Propeller-Nacelle Whirl Flutter

JOHN C. HOUBOLT* AND WILMER H. REED, III**
NASA Langley Research Center

Summary

An analytical investigation is made of a heretofore unimportant flutter phenomenon that may occur in a propeller-nacelle-wing combination—a flutter condition which involves propeller and nacelle precession, and which has been of major concern recently. One of the objects of the investigation is to isolate and show the influence of those parameters which appear to be most strongly linked with this whirl-type instability. Considered, for example, are various combinations of pitch and yaw stiffnesses of the nacelle, structural damping, and propeller speed. To understand the behavior of the system better, the motion due to various initial disturbances is also studied for both subcritical and supercritical conditions.

The results presented are derived by digital and analog means, the analog setup being used primarily for the motion studies. Part of the study is devoted to a further examination of the propeller aerodynamics. Finally, a comparison is made of analytically determined critical conditions with results obtained in some wind-tunnel tests.

Symbols

a = lift-curve slope
a_1, b_1 = generalized coordinates
A = blade aspect ratio
c = blade chord
c_0 = blade reference chord
e = distance between pivot and propeller plane
EI_1, EI_2 = bending stiffnesses in the yaw and pitch directions
F, G = oscillating lift function of flutter
g = structural damping (as used in $1 + ig$ times the stiffness)
i = $\sqrt{-1}$
I_y = total moment of inertia of system about pivot point
J = advance ratio, $\pi V/\Omega R$
k, k_ψ, k_θ = reduced frequency parameters, $k = \omega c_0/2\Omega R$, $k_\psi = \omega_\psi c_0/2\Omega R$, $k_\theta = \omega_\theta c_0/2\Omega R$
k_p = radius of gyration of propeller about a diametrical axis
k_P = radius of gyration of propeller about spin axis
K_ψ, K_θ = effective linear stiffnesses in the yaw and pitch directions (see table in Appendix A)
l = aerodynamic lift on blade per unit length
L_y, L_z = total aerodynamic force due to propeller in the y and z directions
M = forward-flight Mach number
M_p = mass of propeller
M_y, M_z = total aerodynamic moment due to propeller about the y and z axes
M_ψ, M_θ = effective generalized mass in the yaw and pitch directions
n = stiffness ratio, K_ψ/K_θ
r = radius from hub to section along blade
R = blade tip radius
S' = propeller disk area
S_ψ S_θ = torsional spring constant in yaw and pitch directions (see table in Appendix A)
t = time
U = resultant velocity at radius r, $U = \sqrt{V^2 + \Omega^2 r^2}$ (also used for potential energy)
V = forward flight speed
x, y, z = coordinate axes (see Appendix A)
α = angle of attack
β_ψ, β_θ = viscous damping factors in yaw and pitch directions
β_{cr} = critical damping factor, $2\sqrt{K_\psi M_\psi}$
θ = pitch angle
μ = mass ratio, $M_p/\pi\rho c_0^2 R$
ρ = air density in mass units
ϕ = phase angle
ψ = yaw angle
ω = precession frequency
ω_ψ, ω_θ = fundamental natural frequencies in yaw and pitch for nonrotating propeller
Ω = propeller rotational frequency

Introduction

THE PURPOSE OF THIS PAPER is to examine some of the fundamental aspects of the propeller whirl flutter—a precision-type instability that can occur in a flexibly mounted aircraft engine-propeller combination.

Although Browne and Taylor[1] recognized the possible existence of such an instability as early as 1938, it was found that the conditions under which such a system becomes unstable were not likely to be encountered in actual aircraft of that era. The situation did not change in subsequent years and so further consideration of the whirl phenomenon subsided or, at least, was considered to be essentially of academic interest only. However, modern configurations such as turbopropeller aircraft with long-overhang nacelles and unusual VTOL configurations have given rise to a re-examination of the entire problem. Ref. 2 represents a recent consideration of the problem.

This paper attempts to generalize and extend the treatment, and specifically aims to isolate and show the influence of some of the key parameters involved in propeller whirl. The approach followed is to deal primarily with some rather simple systems with a view toward obtaining a better understanding of the basic mechanism of the phenomenon. The body of the paper describes the systems treated, indicates the importance of various parameters on whirl stability, and presents some substantiating experimental data. The analytical procedures used are developed separately in appendices at the end of the paper and in Ref. 2. These appendices include an independent development of the nonsteady

Presented at the Aeroelasticity Session, IAS 29th Annual Meeting, New York, January 23–25, 1961.

* Associate Chief, Dynamic Loads Division.
** Aerospace Technologist.

Reprinted from JOURNAL OF THE AEROSPACE SCIENCES

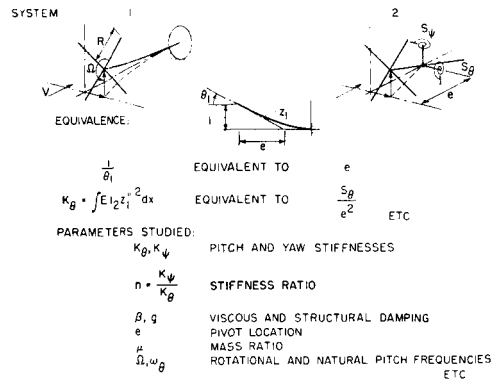

FIG. 1. Systems considered.

propeller aerodynamics involved, including an approximate examination of aerodynamic lag effects.

Dynamic System

Cases Treated

First, let us look at the two cases which we will be treating throughout the paper (Fig. 1). In system 1 on the left, the power plant and nacelle structure are represented by a cantilever beam having a continuous arbitrary distribution of mass and stiffness along its length L. In system 2, a rigid nacelle or power-plant structure is assumed to be spring-restrained about pitch and yaw axes located a distance e behind the propeller disk. (System 2 was the representation used in Ref. 2.) It is assumed that the vibration characteristics of both systems can be described by two degrees of freedom—pitch motion in a vertical plane and yaw motion in a horizontal plane. Pertinent physical properties for the systems to be considered in this paper are given in Table 1.

When the continuous system is approximated by a single natural pitch mode and a single natural yaw mode, as in the present case, equivalent relations can be established between the two systems. For example, an effective pivot location for pitch motion may be defined for system 1 as being simply $1/\theta_1$, where θ_1 is the inclination of the propeller axis corresponding to a unit deflection in the natural pitch mode z_1. Similarly, equivalent stiffnesses, mass properties, and so on can also be derived for the two systems (see Appendix A).

The bottom of Fig. 1 lists a few of the important parameters that have been studied. The parameters include the effective pitch and yaw stiffnesses, K_θ and K_ψ, the stiffness ratio $n = K_\psi/K_\theta$, viscous and structural damping coefficients β and g, the distance e from the propeller plane to the pivot axis, a nondimensional mass parameter μ expressing a ratio of blade structural mass to air mass, the rotational speed Ω of the propeller, and the undamped natural pitch frequency ω_θ of the system with a nonrotating propeller. These and other parameters are defined in more detail in Appendix A, where the equations of motion for the two systems are derived.

Gyroscopic Coupling

Before we discuss the influence of these various parameters on whirl stability, it is instructive to look first at a case where damping and aerodynamic forces on the propeller are neglected. Mounted at the end of a flexible structure, which allows angular deflections, the spinning propeller behaves like a gyroscopic pendulum. If, for example, the system is released from an initial pitch deflection, the resulting angular velocity as the system springs back induces a gyroscopic moment about the yaw axis. This moment, in turn, causes the system to yaw, which induces a pitching moment, and so on. Thus, a very significant characteristic of our system is that the pitch and yaw modes are coupled by the gyroscopic action of the rotating propeller. As a result of this coupling, natural modes, which for a nonrotating propeller occur independently in the vertical or horizontal planes, are now characterized by a precession motion about the axis of the undisturbed system (see, for example, Ref. 3).

Precession Frequencies—Fig. 2 shows a typical example of the manner in which the precession frequencies vary with the speed of the propeller. The case shown is for the system wherein the yaw stiffness is assumed to be twice the pitch stiffness so that at zero propeller speed ($\Omega/\omega_\theta = 0$) the frequency ratio is $\omega_\psi/\omega_\theta = \sqrt{2}$. Note that, as we increase the propeller speed—and thus the gyroscopic coupling—the lower frequency decreases and the higher frequency increases. The sketches on the right of Fig. 2 illustrate the elliptical-shaped paths traced by the propeller hub during precession. We see that the lower frequency mode, referred to here as the backward whirl mode, precesses in a direction opposite to that of propeller rotation, while the higher frequency mode precesses in the direction of propeller rotation, and hence is termed the forward whirl mode. In the results to follow we will find that whirl instability always appears to develop in the backward whirl mode.

Propeller Aerodynamics

In Fig. 2 we saw that the propeller gyroscopic moments caused coupling between the pitch and yaw degrees of freedom. We recognize, however, that this gyroscopic action cannot in itself, lead to a divergent-

TABLE 1
Parameters Used for Various Systems

System	1	2A	2B	2C
$R\psi_1$ or R/e*	0.585	2.65†	1.8	2.76
k_p/R	$1/\sqrt{6}$	0.248	$1/\sqrt{6}$	0.338
k_P/R	$1/\sqrt{3}$	0.352	$1/\sqrt{3}$	0.479
σ_1	1.90	6.77	8.91	2.54
R/c_0	4.5	4.63	4.5	2.96
μ	150	170	Variable	88.8

* $\psi_1 = \theta_1$. † In Fig. 10, e/R and the moment of inertia about the pivot axis are varied.

type whirl instability because the net energy input to the system is zero.* Let us now see what happens when the aerodynamic forces acting on the propeller are taken into account. We find that when the resultant air stream is misaligned from the propeller rotation axis due to, say, an angular displacement or a transverse linear velocity of the propeller axis, certain forces and moments are generated (see the derivation in Appendix B or the work of Ribner[4]). For example, if the axis is deflected in pitch, a vertical lift force and a yawing moment are developed by the propeller which are, for small deflections, proportional to the pitch angle. In addition to angular displacements and transverse velocities, there exist aerodynamic forces proportional to the rate of change in the angular deflection.

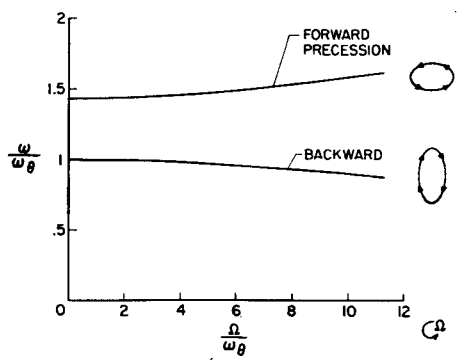

FIG. 2. "Natural" precession frequencies (system 1, $K_\psi = 2K_\theta$).

Propeller Whirl

Stability Boundaries

Conditions of neutral stability of the system may be established as in a conventional flutter analysis by incorporating the propeller aerodynamic terms into the equations of motion and solving for the particular combination of parameters that makes the stability determinant vanish (Appendix A).

Typical Whirl Boundaries—Fig. 3 shows some typical whirl stability boundaries for system 1 plotted in a convenient nondimensional form. The abscissa is the ratio of the airplane forward speed to the propeller tip speed, which is equivalent to $1/\pi$ times the propeller advance ratio J.

Let us direct our attention first to the upper curve which shows the variation of whirl flutter frequency with advance ratio for the case of zero damping. Two points are worth noting. First, since the whirl frequency is less than ω_θ, it is apparent that whirl instability develops in the backward mode. This seems to be a characteristic feature of propeller whirl which has been observed for all systems treated both in the present paper and in Ref. 2. The second point regarding the whirl frequency is that, in general, it is considerably lower than the propeller rotational speed. It is worth noting, therefore, that it appears unlikely that a resonant response in the backward whirl mode would be excited by propeller unbalance forces.

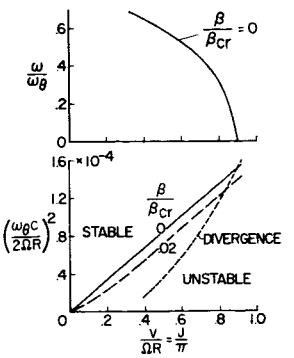

FIG. 3. Whirl stability boundaries (system 1, $K_\psi = 2K_\theta$).

The lower figure shows stability boundaries in which the square of a reduced frequency parameter defined as $\omega_\theta c/2\Omega R$ is plotted against advance ratio J, where ω_θ is the pitch frequency with a stationary propeller, c is a reference propeller blade chord, and ΩR is the tip velocity of the propeller. Note that for a given propeller tip speed the ordinate of the figure is proportional to stiffness in the pitch direction. The area above and to the left of the boundaries indicates the region of stable operation of the system. Propeller whirl boundaries are shown for two damping values—namely, $\beta/\beta_{cr} = 0$ and 0.02. Also plotted on the same figure is the magnitude of the parameter $(\omega_\theta c/2\Omega R)^2$ required to prevent divergence in a static sense. Note that whirl is the critical mode of instability for $V/\Omega R$ values less than 0.8 or 0.9, whereas at somewhat higher values of $V/\Omega R$ system stability is defined by a divergence boundary.

Influence of Various Parameters on Whirl Flutter

Stiffness and Speed Boundaries—The nondimensional stability boundary plots shown in Fig. 3 can be interpreted in various ways. In fact, it is interesting to note just how much information on a system's stability characteristics can be packed into a single plot of this type. By means of illustration, let us apply the results presented in Fig. 3 to the following three cases of practical importance: constant propeller speed, constant advance ratio, and constant stiffness. The first case represents a flight operating condition for a constant-speed propeller. The stiffness airspeed stability boundary for this condition is shown on the left side of Fig. 4. Note that these boundaries are identical in shape to the previously shown nondimensional plot. At the low end of the speed range the stiffness required for stability is

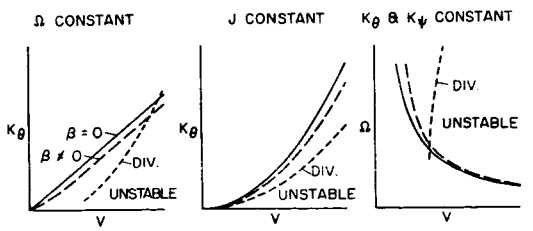

FIG. 4. Illustrative stiffness and speed boundaries (system 1, $K_\psi = 2K_\theta$).

* If the propeller blades are sufficiently flexible, a mechanical instability of the type sometimes encountered in helicopters can occur; however, to preclude mechanical instabilities, only rigid blades are considered in the present analysis.

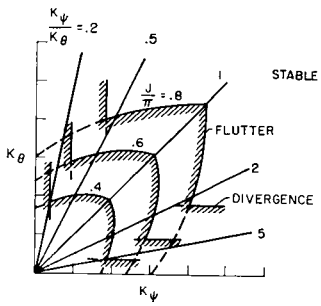

FIG. 5a. Pitch and yaw stiffness required. Effect of advance ratio (system 1, $\beta/\beta_{cr} = 0$).

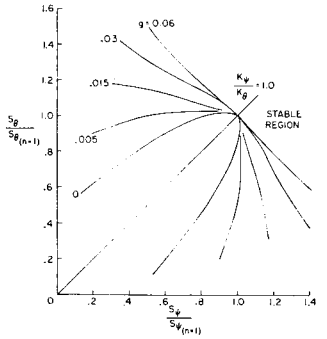

FIG. 5b. Pitch and yaw stiffness required. Effect of damping (system 2A, $J = 1.8$).

low and is governed by propeller whirl flutter; the addition of damping is seen to reduce the amount of stiffness required for stable operation. As speed is increased larger stiffnesses are required for stability, and for sufficiently high speeds stability becomes governed by divergence instead of flutter; damping, of course, does not affect the position of the divergence boundary.

The second case, constant advance ratio, is illustrated by the plot in the center of Fig. 4. This condition corresponds to a windmilling propeller having a fixed blade angle and represents a convenient wind-tunnel test procedure. Again the stability boundaries depict the variation of stiffness required to prevent whirl as a function of airspeed. In this case, however, the curves are parabolas—i.e., K_o is proportional to V^2 or, to put it another way, K_θ varies linearly with dynamic pressure. Note that, in contrast to the previous case, divergence would not be encountered for the particular values of J and damping considered.

Finally, with stiffness held constant, the stability boundaries involving propeller speed and forward speed are illustrated on the right side of Fig. 4. The unstable region is above and to the right. The propeller whirl boundaries for this case are nearly hyperbolic in shape, but for higher values of damping may even curve to the right again with increasing Ω (similar to the divergence curve shown). An important implication of the plot is that for operation on the nearly vertical portion of the curves a large change in propeller speed can occur without altering the critical speed appreciably, but that for operation on the nearly horizontal portion of the curves, the critical speed is quite sensitive to small changes in propeller speed.

Pitch and Yaw Stiffness—Next, let us consider different relative amounts of stiffness in the pitch and yaw directions, as illustrated in Figs. 5a and 5b. Fig. 5a shows the critical pitch stiffness plotted against the critical yaw stiffness for various values of advance ratio. The example treated in this figure is system 1 with zero damping. The whirl and divergence boundaries of interest are indicated by the shaded lines, and the lines radiating from the origin represent lines of constant stiffness ratio. As would be expected, divergence, being a static instability, is governed solely by the minimum of the two stiffnesses involved. Thus, for each value of J/π there corresponds a minimum stiffness level below which the system will diverge. The whirl flutter boundaries, on the other hand, indicate that if the stiffness in one direction is high enough, then the stiffness in

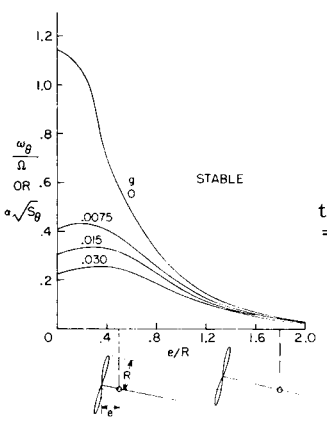

FIG. 7. Effect of pivot location and damping (system 2A, $S_\psi = S_\theta$, $J = 2.6$).

the other direction may even be zero without the system's encountering propeller whirl. This, of course, may be explained by the gyroscopic coupling action which in effect "stiffens" the system in the direction of least stiffness—the system wants to go in the direction of least stiffness but is restrained from going by gyroscopic coupling with the maximum stiffness.

To illustrate the effects of damping, similar whirl flutter boundaries are shown in Fig. 5b for the system treated in Ref. 2 (system 2A). These boundaries were obtained graphically from Fig. 10 of Ref. 2, for an advance ratio of 1.8. The pitch and yaw stiffnesses at each damping value have been normalized with respect to the critical stiffness for the symmetric condition ($n = 1.0$).

A point to be noted in Fig. 5b is that the shape of the whirl boundaries is critically dependent upon the internal damping of the system. In the past, investigators have used—as a simple means of correlating stability boundaries for systems having various stiffness ratios—the concept of an "effective" stiffness, such as the maximum of the two stiffnesses involved, or the rms stiffness defined as $\sqrt{(K_{max}^2 + K_{min}^2)/2}$. (Whirl boundaries described by the maximum stiffness would

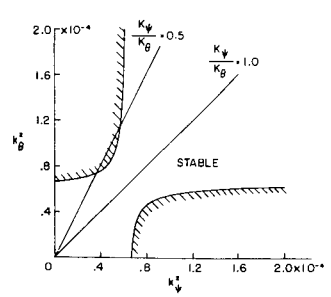

FIG. 6a. Static characteristics. Divergence boundaries (system 1, $J/\pi = 0.6$).

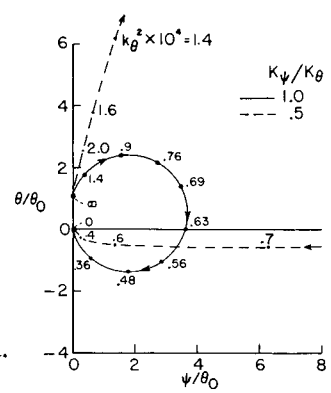

FIG. 6b. Loci of deflections as k_θ^2 is reduced.

plot as a square with sides parallel to the ordinates in Fig. 5, whereas boundaries described by an rms stiffness would plot as a quarter-circle centered at the origin.) Since each of the boundaries presented in Fig. 5b appears to have a different characteristic shape, it is apparent that no simple stiffness criterion is generally applicable over the range of damping values and stiffness ratios shown.*

Static Divergence—It is of interest to consider in somewhat more detail the static-divergence boundaries for a windmilling propeller plotted in Fig. 5a as a function of stiffness in the pitch and yaw directions. The boundaries for $J/\pi = 0.6$ in Fig. 5a have been replotted and extended to zero stiffness in Fig. 6a. (These boundaries are plotted against nondimensional stiffnesses k_θ^2 and k_ψ^2 instead of K_θ and K_ψ as in Fig. 5a.) Note from the corridor of stable operation that if the pitch angle and yaw stiffnesses are equal or nearly equal ($K_\psi/K_\theta \approx 1.0$) the system will be statically stable even when the stiffnesses are reduced to zero. Although in a

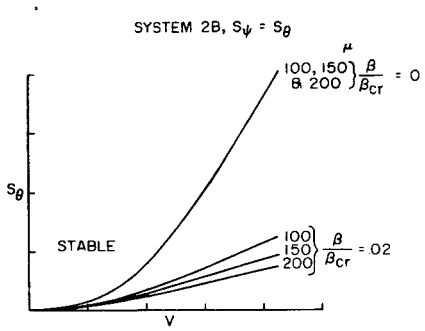

FIG. 8. Effect of mass ratio $\mu = M_p/\pi\rho c_0^2 R$ (system 2B, $K_\psi = K_\theta$).

practical case the critical stiffness of such systems would be governed by whirl-flutter rather than static-divergence considerations, it is instructive, nevertheless, examine the static behavior of a system as stiffness is varied.

For this purpose, consider the situation where a rigidly mounted power plant is inclined at a small pitch angle θ_0 relative to the free stream. Now, let the power-plant mount stiffness be reduced, and observe the static deflections that result. Because of the inclined flow angle, aerodynamic lift and moment develop, causing the system to be deflected both in pitch and in yaw. These deflections bring about changes in the aerodynamic forces, which in turn further modify the deflections. If, however, the system is statically stable, there is associated with each stiffness level a particular combination of pitch and yaw deflections for which the aerodynamic forces acting on the propeller are exactly balanced by the elastic forces developed in the mount system.

In Fig. 6b the loci of this static equilibrium are plotted as the stiffness of the initially rigid system is

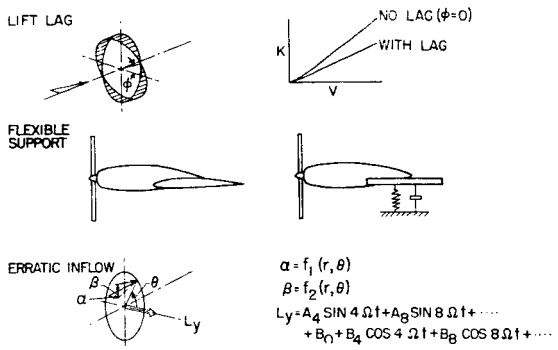

FIG. 9. Additional aspects relating to propeller whirl.

progressively reduced. The two curves shown are for stiffness variations along the $K_\psi/K_\theta = 1.0$ and $K_\psi/K_\theta = 0.5$ lines indicated in Fig. 6a. Whereas Fig. 6a shows the divergence boundaries, Fig. 6b shows the static deformations of the system as these boundaries are approached along lines of constant stiffness ratio. Note that over the limited range of stiffnesses where the $K_\psi/K_\theta = 0.5$ line falls on the unstable side of the divergence boundary, the static deflections in Fig. 6b become infinite. On the other hand, when $K_\psi/K_\theta = 1.0$ the system is statically stable regardless of the stiffness level. Thus, for each reduction in stiffness, the symmetric system—which was initially inclined in pitch relative to the free stream—assumes a finite static pitch and yaw angle of equilibrium as illustrated in Fig. 6b.

Attempts were made to verify the above theoretical predictions in a simple wind-tunnel test for divergence on a symmetric system. A wind-milling propeller was attached to the upstream end of a horizontal rod which was pivoted at the center of gravity of the combination. A large amount of viscous damping was introduced into the system in order to suppress whirl flutter. Contrary to the predictions shown in Fig. 6, a static-type divergence was encountered during the test. Thus, it appears that aerodynamic forces not considered important in propeller whirl can become important in the static-divergence problem. Two such forces that were neglected in the present analysis are the braking action of a windmilling propeller and the aerodynamic-drag forces on the hub and blades of the propeller. More insight into static-divergence aspects is needed.

Pivot Location and Damping—Two other parameters found to play an important role in propeller whirl are the location of the pivot axes and damping. The effect of these parameters on whirl can be illustrated by Fig. 7, which shows the variation of the ratio of pitch frequency to propeller speed ω_θ/Ω with the pivot axis location e/R for various damping values. In varying the

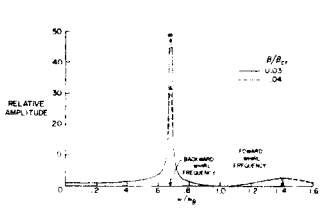

FIG. 10. Frequency response for critical and subcritical conditions on damping (system 2A, $S_\theta = S_\psi$, $J = 1.8$, $e/R = 0.378$).

* These findings are the result of comments by R. E. Donham and E. E. Postel of Lockheed Aircraft Corporation, California Division.

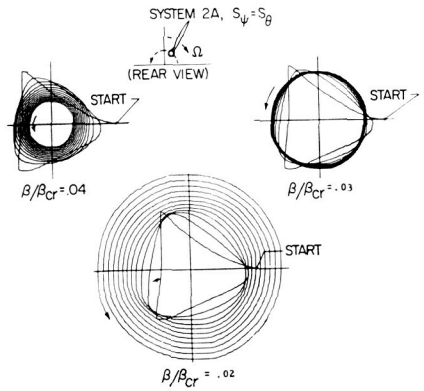

FIG. 11. Transient response for subcritical, critical, and supercritical conditions on damping (system 2A, conditions same as in Fig. 10).

pivot location, appropriate changes were also made in the moments of inertia, so as to represent a fixed mass system. (A structural-type damping is assumed in this case, as in Ref. 2.) For constant propeller speed the ordinate of the figure may be interpreted as being proportional to the square root of the stiffness. An important point to note is that for the smaller e/R values high stiffness is required, and further that the whirl boundaries are rather sensitive to damping changes, especially when the damping is near zero. The further the pivot location is moved from the propeller disk, the less the stiffness required and the smaller the effects of damping. The favorable effect shown by increasing the pivot distance e may be attributed to the aerodynamic damping associated with transverse velocities of the propeller hub—that is, when the pivot is close to the propeller the transverse velocities due to precession are small and as a result the aerodynamic damping is small relative to the structural damping. With a large pivot distance, however, the aerodynamic damping tends to predominate and therefore causes the system to be less sensitive to changes in structural damping.

Effect of Mass Ratio—Consider next the effect of varying a mass ratio parameter defined as $\mu = M_p \div \pi\rho c_0^2 R$. This parameter is a measure of the propeller blade mass relative to a cylindrical mass of air surrounding the blade. Fig. 8 shows the effect of μ on the stiffness-velocity boundaries for damping values $\beta/\beta_{cr} = 0$ and 0.02. When damping is zero, variations in μ have a negligible influence on the boundaries. With a damping of $\beta/\beta_{cr} = 0.02$, however, we see the required stiffness is lowered with increasing μ. A μ increase can be associated with an increase in flight altitude, in which case one might anticipate the trends indicated in Fig. 8 because of the reduced magnitude of the aerodynamic forces acting on the propeller.

Additional Aspects—Let us now briefly discuss three additional aspects of propeller whirl (Fig. 9). The first effect indicated is the effect of lag in lift developed by the propeller blades. As an illustration, consider the propeller axis to be deflected in yaw relative to the free stream. The angle of attack of each blade element therefore varies sinusoidally once per revolution of the propeller, being zero for the horizontal position and maximum for the vertical position. From a quasi-steady point of view the lift should be in phase with this sinusoidal variation in angle of attack. As a consequence of wake effects, however, the unsteady lift force on a blade element lags the angle of attack by a phase angle ϕ (see Appendix B). In most of the results presented in this paper aerodynamic phase lag has been ignored. The sketch in the upper right of Fig. 9 is presented, however, to illustrate the effect of lift lag on the stiffness-speed whirl boundary. It can be seen that aerodynamic phase lag tends to have a stabilizing effect on the system.

Next, let us ask what effect wing flexibility has upon whirl stability. Actually, the answer to this question is beyond the scope of the paper; however, certain general remarks and speculations can be offered.

Limited experimental and analytical evidence suggests that the effect of adding a propeller-nacelle combination to a wing tends to have a stabilizing effect on the whirl flutter mode—that is, the speed necessary to cause whirl instability for the wing-mounted case is greater than the critical speed for the rigidly mounted nacelle. The wing in this instance, therefore, seems to act primarily as a damped-mass oscillator, capable of absorbing energy, as is depicted by the right-hand middle sketch of Fig. 9.

On the other hand, if the wing by itself has a flutter speed approximately equal to the critical speed for the rigidly mounted nacelle, the combination of the two might conceivably cause a lowering of the flutter speed. Also, if the wing by itself has a flutter speed less than the critical speed for the rigidly mounted nacelle, the addition of the nacelle to the wing might cause the wing to be stabilized. Further work is needed, however, to verify and elaborate on these points.

Finally, we show at the bottom of Fig. 9 the effects of an erratic inflow distribution over the propeller disk. Such an inflow could be produced by flow irregularities over the fuselage or other bodies in the vicinity of the propeller. We wish to examine whether the aerodynamic loads associated with such an inflow can excite a resonant response in the whirl mode at subcritical conditions. To do this, assume an inflow distribution which is an arbitrary function of position on the pro-

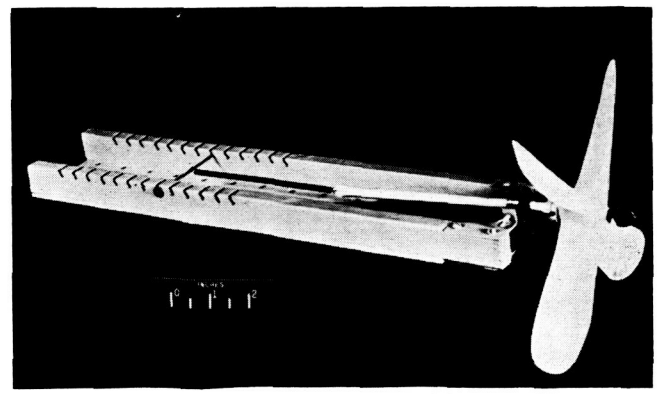

FIG. 12. Propeller whirl model tested.

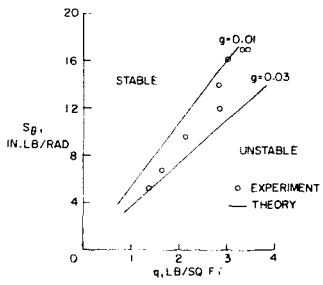

FIG. 13. Experimental propeller whirl boundaries.

peller disk but does not vary with time. It can be shown by Fourier-series development that the fundamental frequency component of the loads associated with such an inflow is equal to the propeller speed times the number of blades—in this case, say, 4Ω—and that the higher harmonics are integral numbers of this fundamental frequency. This frequency is well above the whirl frequency for any practical configurations that can be envisioned. Hence, erratic inflow is not expected to excite a forced-type resonant response of propeller whirl mode. However, if the disturbance is a function of time, such as would be the case with a gust, or if nonlinear effects arise, forced response in the whirl mode may become a question of practical importance.

Subcritical and Supercritical Response

Frequency Response

Figs. 10 and 11 illustrate some response characteristics of the system as the critical whirl boundary is approached by varying damping. We first consider the frequency response of system 2A due to a sinusoidal moment applied about the pitch axis, for $S_\theta = S_\psi$. Curves are shown for two damping values representing stable ($\beta/\beta_{cr} = 0.04$) and neutrally stable ($\beta/\beta_{cr} = 0.03$) conditions. The frequency scale has been normalized with respect to ω_θ and the ordinate with respect to θ_{static}. As pointed out earlier, the unstable mode develops from the backward whirl mode, as is evidenced by the fact that the frequency is less than ω_θ. Note also that the forward mode, having a frequency greater than ω_θ, is well-damped both for the subcritical and critical conditions.

Transient Response

In Fig. 11 transient responses as obtained on an analog computer are shown for the same system considered in Fig. 10. Here the propeller response is viewed from behind and it is rotating in a clockwise sense. The curves represent paths traced by the propeller hub subsequent to an initial lateral displacement to the right. The top two figures represent stable and neutrally stable conditions and are for the same damping values used in Fig. 10. The bottom curve is for a slightly smaller damping ($\beta/\beta_{cr} = 0.02$) and, as can be seen, represents the diverging motion of an unstable system.

Here again it can be observed that the instability develops in the backward whirl mode, by noting that the system is precessing in a counterclockwise direction, whereas the propeller is rotating clockwise. Evidence of the forward mode, which is also excited by the initial condition used, can be seen from corners formed in the path during early stages of the transient motion. This mode quickly dampens out, however, as would be expected from indications shown in the previous frequency response plots.

Experimental Results

Up to this point all of the results presented have been based entirely on theoretical considerations. In this concluding section some experimental data are presented which tend to bear out some of the predicted trends. These results were obtained in a small open-throat wind tunnel at speeds between 30 and 50 ft/sec.

Model Tested

A photograph of the model tested is shown in Fig. 12. It consists of a windmilling propeller attached to a rod which has freedom to pitch and yaw about a set of gimbal axes. The stiffness is controlled by varying the tension in a spring connected axially to the other end of the rod. Note that the model represents system 2 and has equal pitch and yaw stiffnesses. Pertinent parameters for the model are tabulated in Table 1 under system 2C.

Model Stability Boundaries

The results of the wind-tunnel tests are given in Fig. 13, which shows the stiffness required for neutral stability plotted against dynamic pressure. It will be recalled from Fig. 4 that theory predicts a linear variation of stiffness with dynamic pressure q for a windmilling propeller (J constant). In general, the experimental results support this conclusion. Damping measurements before and after the tests were not always repeatable, but generally fell between $g = 0.02$ and $g = 0.05$. It can be seen that the experimental-data points fall within the theoretical boundaries computed for $g = 0.01$ and $g = 0.03$ damping. Further propeller-whirl tests under somewhat better-controlled conditions than were possible here are being considered.

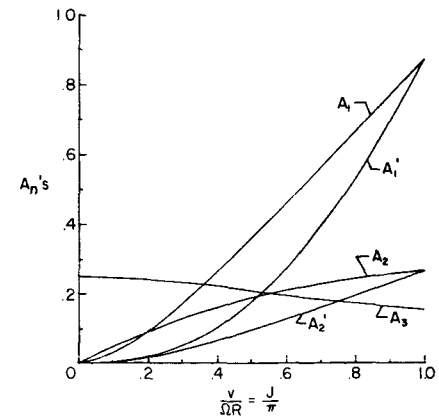

FIG. 14. Nonsteady aerodynamic coefficients for constant chord propellers (nonthrusting).

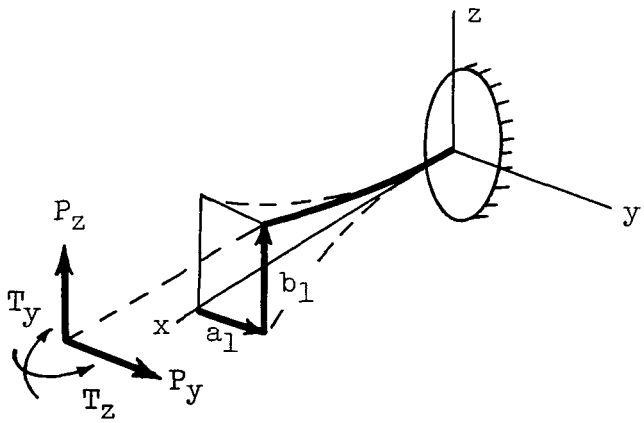

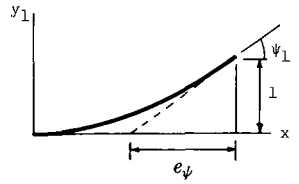

SKETCH A. (Left).

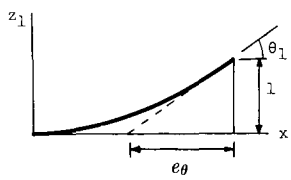

SKETCH B. (Right).

Concluding Remarks

From the consideration of whirl flutter that has been made herein the following basic conclusions may be drawn.

(1) In general, whirl flutter is strongly dependent on the stiffness, the damping, and the pivot location.

(2) The concept of an "effective" stiffness for systems having unequal pitch and yaw stiffnesses should be used with caution, because the shapes of the stiffness boundaries depend strongly upon other system characteristics, particularly damping, and appear to preclude the use of any single criterion.

(3) Experimental data presented herein tend to confirm the analytical results.

In concluding, it is appropriate to call attention to a few propeller whirl parameters not considered in this paper. The effects of some of these parameters were investigated in Ref. 2 and may be summarized as follows.

(1) Mach-number effects tend to be slightly destabilizing.

(2) Propeller-thrust effects can be ignored (as deduced from cruise-flight conditions only).

(3) Structural-type damping and viscous-type damping give different stability boundaries.

(4) When damping in pitch and yaw are unequal, it is beneficial to have the greater damping in the direction of minimum stiffness.

Additional important factors are almost certain to arise in the treatment of more complex systems. One might find cases, for example, where added degrees of freedom, such as propeller blade flexibility, produce significant changes in the stability of a system. The study of this and other propeller whirl systems having more than two degrees of freedom would be a logical extension to the work treated herein.

Appendix A
Derivation of Equations for Whirl Instability

System Dynamics

Cantilevered System—In this system the propeller-nacelle-engine combination is considered to be attached at the aft end of the nacelle to a rigid support as a cantilever beam. The system is thus capable of deflecting as shown in Sketch A, in which the forces and moments due to the propeller are shown as arrows. The governing equation of motion may be derived by the Lagrangian dynamic equation approach. Thus, assume the deflections in the y- and z-directions to be expressed in terms of chosen modal functions as

$$y = a_1 y_1, \qquad z = b_1 z_1 \tag{A1}$$

where the modal functions have the characteristics shapes illustrated schematically in Sketch B.

The slopes or rotations at the cantilever tip would be

$$\left.\begin{aligned} \psi &= (dy/dx)_{x=L} = a_1\psi_1 \\ \theta &= (dz/dx)_{x=L} = b_1\theta_1 \end{aligned}\right\} \tag{A2}$$

With Eqs. (A1) and (A2), the kinetic energy, potential energy, and virtual work expressions thus may be written

$$T = \frac{1}{2}\int_0^L m_e \dot{a}_1^2 y_1^2 dx + \frac{1}{2}\int_0^L m_e \dot{b}_1^2 z_1^2 dx$$

$$U = \frac{1}{2}\int_0^L EI_1 a_1^2 y_1''^2 dx + \frac{1}{2}\int_0^L EI_2 b_1^2 z_1''^2 dx$$

$$\delta W = \delta a_1 P_y + \delta a_1 \psi_1 T_z + \delta b_1 P_z + \delta b_1 \theta_1 T_y$$

where m_e is the mass per unit length of the nacelle and engine, EI_1 and EI_2 are the bending stiffnesses in the y- and z-directions, and a prime and a dot denote derivations with respect to x and time t, respectively.

From Lagrange's dynamic equation

$$(d/dt)(\partial T/\partial \dot{q}_n) + (\partial U/\partial q_n) = Q_n = (\delta W/\delta q_n)$$

the equations of motion follow as

$$M_1\ddot{a}_1 + K_\psi a_1 = P_y + \psi_1 T_z$$

$$M_2\ddot{b}_1 + K_\theta b_1 = P_z + \theta_1 T_y$$

where

$$\left.\begin{aligned} M_1 &= \int_0^L m_e y_1^2 dx, \quad K_\psi = \int_0^L EI_1 y_1''^2 dx \\ M_2 &= \int_0^L m_e z_1^2 dx, \quad K_\theta = \int_0^L EI_2 z_1''^2 dx \end{aligned}\right\} \tag{A3}$$

Structural damping may be taken into account by introducing either a viscous or a "complex" type damping term in each equation—for example, either $\beta_\psi \dot{a}_1$ or $(1 + ig)K_\psi$ in the first equation. This derivation will be limited to viscous-type damping; the modified equations therefore appear

$$\left.\begin{aligned} M_1\ddot{a}_1 + \beta_\psi \dot{a}_1 + K_\psi a_1 &= P_y + \psi_1 T_z \\ M_2\ddot{b}_1 + \beta_\theta \dot{b}_1 + K_\theta b_1 &= P_z + \theta_1 T_y \end{aligned}\right\} \tag{A4}$$

A separation of the forces and moments at the propeller hub into inertial and aerodynamic components is convenient at this point. The propeller is considered to be rotating counterclockwise with angular velocity Ω when viewed from the front. The consideration, then, of the inertia forces and moments due to translation and rotation (through d'Alembert's principle), and the basic right-hand rule for a gyroscope (Sketch C)—i.e., in terms of the motion given by Eqs. (A1) and (A2)—leads to the following equations:

$$P_y = -M_p\ddot{a}_1 + L_y, \qquad P_z = -M_p\ddot{b}_1 + L_z$$

$$T_z = -M_pk_p^2\ddot{a}_1\psi_1 - M_pk_P^2\Omega\dot{b}_1\theta_1 + M_z$$

$$T_y = -M_pk_p^2\ddot{b}_1\theta_1 + M_pk_P^2\Omega\dot{a}_1\psi_1 + M_y$$

where M_p is the mass of the propeller, k_p and k_P are the radii of gyration of the propeller about a diameter and about the spin axis, respectively, and L_y,L_z and M_z,M_y are the aerodynamic forces and moments exerted by the propeller at the hub. The substitution of these equations into Eqs. (A4) gives

$$\left.\begin{aligned} M_\psi\ddot{a}_1 + \beta_\psi\dot{a}_1 + K_\psi a_1 + M_pk_P^2\theta_1\psi_1\Omega\dot{b}_1 &= \\ L_y + \psi_1M_z & \\ -M_pk_P^2\theta_1\psi_1\Omega\dot{a}_1 + M_\theta\ddot{b}_1 + \beta_\theta\dot{b}_1 + K_\theta b_1 &= \\ L_z + \theta_1M_y & \end{aligned}\right\} \quad (A5)$$

where

$$M_\psi = M_1 + M_p + M_pk_p^2\psi_1^2$$

$$M_\theta = M_2 + M_p + M_pk_p^2\theta_1^2$$

A gyroscopic coupling of the equations of motion is thus seen to occur, a fact which is of fundamental importance to the establishment of whirl. In fact, when the right-hand sides are set equal to zero, the resulting homogeneous equation leads to natural modes which are characteristically of the precession type (Fig. 2). A subsequent section will introduce the aerodynamic forces and moments of the propeller (which adds further coupling) to establish the complete dynamic equations governing the whirl phenomenon for the system under consideration.

Pivoting System—Another representation that can be envisioned for a propeller-nacelle combination is to have the propeller and at least part of the engine act as a rigid unit which is pivoted or gimbaled at some point along the engine axis, the motion being restrained by pitch and yaw springs. Such a system is illustrated schematically in Sketch D. Here the generalized coordinates of motion may be a_1 and b_1 as used in the previous section, or θ and ψ, the connection being

$$a_1 = e\psi, \qquad b_1 = e\theta \quad (A6)$$

For comparison with the previous section, a_1 and b_1 will be used. By use of a procedure analogous to that used in the preceding section, it may be shown that the equations governing the motion of this pivoting type system are as follows

$$\left.\begin{aligned} \frac{I_y}{e^2}\ddot{a}_1 + \beta_\psi\dot{a}_1 + \frac{S_\psi}{e^2}a_1 + M_pk_P^2\frac{1}{e^2}\Omega\dot{b}_1 &= \\ L_y + \frac{1}{e}M_z & \\ -M_pk_P^2\frac{1}{e^2}\Omega\dot{a}_1 + \frac{I_y}{e^2}\ddot{b}_1 + \beta_\theta\dot{b}_1 + & \\ \frac{S_\theta}{e^2}b_1 = L_z + \frac{1}{e}M_y & \end{aligned}\right\} \quad (A7)$$

where I_y is the total mass moment of inertia about the pivot point defined by

$$I_y = M_ek_e^2 + M_pe^2 + M_pk_p^2$$

in which M_e is the mass pivoting about the pivot point excluding the propeller, and k_e is the radius of gyration of this mass about the pivot location.

Equivalence of Cantilever and Pivoting Systems—Through comparison of Eqs. (A5) and (A7), a means is afforded for expressing the parameter of one system in terms of those of the other system. The key point in this comparison is the recognition that the extension of the end slope of a chosen modal function leads to an intersection with the x-axis which corresponds to the pivot location (see Sketch B).

The fact that ψ_1 and θ_1 may be different means that the pivot point for yaw is different than that for pitch. In this comparison, however, the following equalities will be assumed: $\psi_1 = \theta_1$ and $y_1 = z_1$. The relations which express the equivalence of the two systems may then be listed as follows:

Replace	By
$\psi_1 = \theta_1$	$1/e$
$M_\psi = M_\theta$	I_y/e^2
K_ψ	S_ψ/e^2
K_θ	S_θ/e^2

Equations for Whirl Flutter

In Appendix B the equations for the aerodynamic forces and moments of a precessing propeller are derived [Eqs. (B8)]. If these are substituted into Eqs. (A5), using Eqs. (A2), and if the following complex sinusoidal motion is assumed

$$a_1 = a_{10}e^{i\omega t}, \qquad b_1 = b_{10}e^{i\omega t}$$

a pair of homogeneous equations will be obtained which define conditions at whirl instability. The determinant of these equations may be shown to be of the form

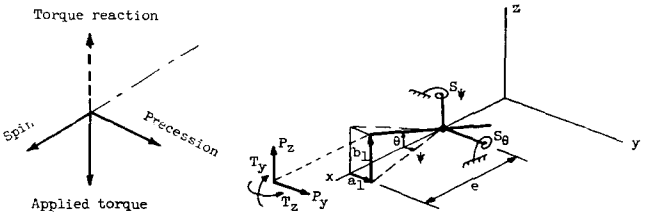

SKETCH C. (Left). SKETCH D. (Right).

$$\begin{vmatrix} \sigma_1(k_\psi^2 - k^2) - a_0 + k(b_0 + \delta_1)i & -c_1 + k(d_1 + e_1)i \\ c_1 + k(d_1 - e_1)i & \sigma_2(k_\theta^2 - k^2) - a_2 + k(b_2 + \delta_2)i \end{vmatrix} = 0 \qquad \text{(A8)}$$

where

$$k = \omega c_0/2\Omega R, \quad k_\psi = \omega_\psi c_0/2\Omega R, \quad \omega_\psi^2 = K_\psi/M_\psi$$

$$k_\theta = \omega_\theta c_0/2\Omega R, \quad \omega_\theta^2 = K_\theta/M_\theta$$

$$\sigma_1 = M_\psi/M_p = (M_1/M_p) + 1 + k_p^2\psi_1^2$$

$$a_0 = \psi_1 c_0 A_1'/2\mu, \quad b_0 = (A_1 + \psi_1^2 R^2 A_3)/\mu$$

$$c_1 = (\psi_1\theta_1 R c_0 A_2')/2\mu, \quad d_1 = [(\psi_1 - \theta_1)RA_2]/\mu$$

$$\mu = M_p/4M_a = M_p/\pi\rho c_0^2 R, \quad e_1 = (c_0/2R)\psi_1\theta_1 k_P^2$$

$$\delta_1 = 2(\beta_\psi/\beta_{cr})\sigma_1 k_\psi, \quad \delta_2 = 2(\beta_\theta/\beta_{cr})\sigma_1 k_\psi$$

$$\beta_{cr} = 2\sqrt{K_\psi M_\psi}, \quad \sigma_2 = M_\theta/M_p = (M_2/M_p) + 1 + k_p^2\theta_1^2$$

$$a_2 = (\theta_1 c_0 A_1')/2\mu, \quad b_2 = (A_1 + \theta_1^2 R^2 A_3)/\mu$$

and where the factors A_1, A_1', etc., are propeller functions which are derived in Appendix B. For a given propeller they depend only on the advance ratio J—see, e.g., Fig. 14.

Eq. (A8) represents a complex characteristic equation which defines whirl instability or "whirl flutter," and solution to the equation proceeds in the same manner as is used in flutter work. Note that a reduced frequency k based on the rotational tip speed of the propeller appears as a natural parameter, and that a mass ratio μ in terms of the propeller blade mass and the mass of a cylinder of air surrounding the blade has been used.

In application to specific cases, one procedure for the solution of Eq. (A8) is to consider all system parameters known except the stiffness level necessary to prevent instability; the relative stiffness in the pitch and yaw directions may be specified, say $K_\psi = nK_\theta$ (which means that $k_\psi^2 = nk_\theta^2$). Then for a chosen value of $V/\Omega R$, solution is performed for k and k_θ^2. Trial-and-error solutions are avoided by algebraically solving the imaginary part of the determinant for k^2 in terms of k_θ^2, ignoring the fact that the damping terms are functions of k_ψ—that is, assuming that δ_1 and δ_2 are in the nature of known values. This equation for k^2 is then substituted into the real part to give a quadratic equation in k_θ^2 alone, which is readily solvable. In the solution for k_θ^2, damping is handled by simply assigning values to δ_1 and δ_2. After the solution is obtained, the values of damping which would lead to the assigned values of δ_1 and δ_2 are found by inverting the equations defining the δ's—for example, $\beta_\psi/\beta_{cr} = \delta_1/2\sigma_1 k_\psi$. For cases having certain symmetries much simplification to this solution results. In fact, for the case of $\psi_1 = \theta_1$, $M_1 = M_2$, $\beta_\psi = \beta_\theta$ (note $\psi_1 = \theta_1$ makes $d_1 = 0$), and for the notation $K_\psi = nK_\theta$ or $k_\psi^2 = nk_\theta^2$, the quadratic is

$$\sigma_1^2\left(\frac{n-1}{2}\right)^2 k_\theta^4 + \frac{n+1}{2}[(b_0 + \delta_1)^2 + e_1^2]k_\theta^2 - [(b_0 + \delta_1)^2 + e_1^2]\left[\frac{a_0}{\sigma_1} + \frac{c_1 e_1}{\sigma_1(b_0 + \delta_1)} + \frac{c_1^2}{(b_0 + \delta_1)^2}\right] = 0$$

For the special case of equal stiffnesses in both the yaw and pitch directions ($n = 1$), the solution of Eq. (A8) is simplified even more, and is

$$k = c_1/(b_0 + \delta_1)$$

$$k_\theta^2 = k^2 + (a_0/\sigma_1) + k(e_1/\sigma_1)$$

Appendix B

Propeller Aerodynamics

Section Displacements and Velocities

Consider a rotating propeller undergoing a precession or "whirl" about its spin axis. The position at any instant may be represented by the head-on sketch, Sketch E.

In addition to the displacements indicated, the propeller plane will yaw a small amount ψ about a line parallel to the z-axis and will pitch an amount θ about a line parallel to the y-axis. (For the cantilever type of nacelle deformation considered in Appendix A, these rotations are

$$\psi = a_1\psi_1, \qquad \theta = b_1\theta_1$$

while for the pivoting system these rotations are a_1/e and b_1/e, respectively.)

A first-order approximation to the nonsteady aerodynamic forces that develop on the precessing propeller can be developed by a strip-theory approach. Basic in this consideration are three perturbation quantities: the local or section geometric angle-of-attack change, the perturbation velocity $\dot{s}$ in the propeller plane, and the perturbation velocity $\dot{w}$ out of the propeller plane.

Consider blade 1: the geometric angle-of-attack change along the blade due to yaw ψ and pitch θ is

$$\alpha_1 = \psi \sin \Omega t - \theta \cos \Omega t \qquad \text{(B1)}$$

The perturbation velocities $\dot{s}$ and $\dot{w}$ of a point situated at radius r can be determined from the equations describing the instantaneous position of this point:

$$y = a_1 + r \cos \Omega t$$

$$z = b_1 + r \sin \Omega t$$

$$w_1 = -\psi r \cos \Omega t - \theta r \sin \Omega t$$

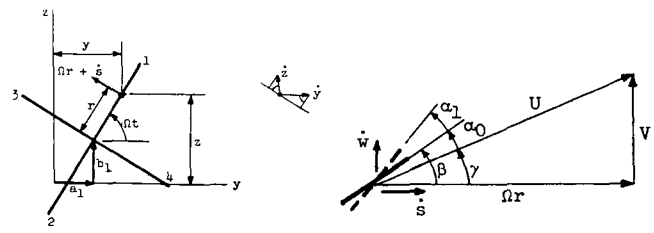

SKETCH E. (Left). SKETCH F. (Right).

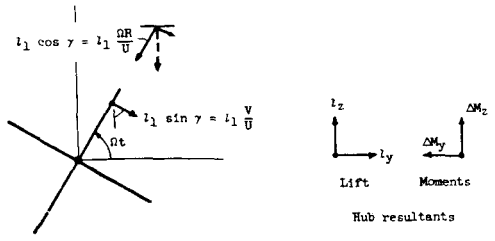

SKETCH G.

Thus

$$\left.\begin{aligned} \dot{s} &= -\dot{y}\sin\Omega t + \dot{z}\cos\Omega t - \Omega r \\ &= -\dot{a}_1\sin\Omega t + \dot{b}_1\cos\Omega t \\ \dot{w} &= -\dot{\psi}r\cos\Omega t + \psi r\Omega\sin\Omega t - \\ &\qquad \dot{\theta}r\sin\Omega t - \theta r\Omega\cos\Omega t \end{aligned}\right\} \quad \text{(B2)}$$

Section Lift

The nonsteady lift that develops on a section of blade 1 may be established from α_1, $\dot{s}$, $\dot{w}$ of the preceding section through use of Sketch F, where β represents the steady-state blade angle. The velocities $\dot{s}$ and $\dot{w}$ lead to a velocity component normal to the resultant velocity U of magnitude

$$-\dot{w}(\Omega r/U) + \dot{s}(V/U)$$

With α_1 and this normal velocity the effective angle of attack sensed by the blade is

$$\alpha = \alpha_0 + \alpha_1 - \dot{w}(\Omega r/U^2) + \dot{s}(V/U^2)$$

The velocities $\dot{s}$ and $\dot{w}$ also lead to a component in the direction of U and thus cause the effective resultant velocity to be

$$U_e = U + \dot{w}(V/U) + \dot{s}(\Omega r/U)$$

The lift that develops on the blade is therefore

$$\begin{aligned} l &= (a/2)\rho c U_e^2 \alpha \\ &= \frac{a}{2}\rho c(U^2 + 2\dot{w}V + 2\dot{s}\Omega r)\times \\ &\qquad \left(\alpha_0 + \alpha_1 - \dot{w}\frac{\Omega r}{U^2} + \dot{s}\frac{V}{U^2}\right) \\ &= \frac{a}{2}\rho c U^2\left[\alpha_0 + \alpha_1 - \frac{\Omega r}{U^2}\left(1 - \frac{2V}{\Omega r}\alpha_0\right)\dot{w} + \right. \\ &\qquad \left. \frac{V}{U^2}\left(1 + \frac{2\Omega r}{V}\alpha_0\right)\dot{s}\right] \quad \text{(B3)} \end{aligned}$$

where a is the section left-curve slope and c the blade chord. The first term in brackets is associated with the steady-state lift while the remaining terms lead to the nonsteady lift effects. Note that the nonsteady lift terms involving $\dot{w}$ and $\dot{s}$ are influenced by the steady-state angle of attack α_0. The terms $(2V/\Omega r)\alpha_0$ and $(2\Omega r/V)\alpha_0$ are generally small compared to the unit values shown, however, and therefore contribute very little to the lift; indeed, for a nonthrusting (windmilling) propeller, where $\alpha_0 = 0$, they vanish. They are therefore neglected in the remainder of the paper.

With α_0 considered zero, the substitution of Eqs. (B1) and (B2) into Eq. (B3) gives the following equations for the nonsteady lift that develops on blade 1:

$$\begin{aligned} l_1 &= -(a/2)\rho c(V^2\theta - V\dot{b}_1 - \Omega r^2\dot{\psi})\cos\Omega t + \\ &\qquad (a/2)\rho c(V^2\psi - V\dot{a}_1 + \Omega r^2\dot{\theta})\sin\Omega t \\ &= -f_1\cos\Omega t + f_2\sin\Omega t \end{aligned} \quad \text{(B4)}$$

The section lift on the other blades is found readily from this equation by replacing

Ωt by $\Omega t + \pi$ for blade 2

Ωt by $\Omega t + (\pi/2)$ for blade 3

Ωt by $\Omega t + (3\pi/2)$ for blade 4

With this substitution it is found that

$$\left.\begin{aligned} l_2 &= -l_1 \\ l_3 &= (a/2)\rho c(V^2\theta - V\dot{b}_1 - \Omega r^2\dot{\psi})\sin\Omega t + \\ &\qquad (a/2)\rho c(V^2\psi - V\dot{a}_1 + \Omega r^2\dot{\theta})\cos\Omega t \\ &= f_1\sin\Omega t + f_2\cos\Omega t \\ l_4 &= -l_3 \end{aligned}\right\} \quad \text{(B5)}$$

Propeller Side Forces and Moments

To determine the side forces and moments of the nonsteady propeller aerodynamics it is convenient to resolve the section lift force into torque and thrust components as depicted in Sketch G. These components lead to side forces l_y and l_z in the y- and z-directions and to moments ΔM_z and ΔM_y about the z- and y-axes. The equations for these quantities are found [with the use of Eqs. (B5)] to be

$$\left.\begin{aligned} l_y &= 2(V/U)(l_1\sin\Omega t + l_3\cos\Omega t) \\ l_z &= 2(V/U)(-l_1\cos\Omega t + l_3\sin\Omega t) \\ \Delta M_z &= r(\Omega r/V)l_z \\ \Delta M_y &= -r(\Omega r/V)l_y \end{aligned}\right\} \quad \text{(B6)}$$

With Eqs. (B4) and (B5) these equations become

$$\left.\begin{aligned} l_y &= a\rho c(V/U)(V^2\psi - V\dot{a}_1 + \Omega r^2\dot{\theta}) = \\ &\qquad 2(V/U)f_2 \\ l_z &= a\rho c(V/U)(V^2\theta - V\dot{b}_1 - \Omega r^2\dot{\psi}) = \\ &\qquad 2(V/U)f_1 \\ \Delta M_z &= a\rho cr(\Omega r/U)(V^2\theta - V\dot{b}_1 - \Omega r^2\dot{\psi}) = \\ &\qquad 2(\Omega r^2/U)f_1 \\ \Delta M_y &= -a\rho cr\frac{\Omega r}{U}(V^2\psi - V\dot{a}_1 + \Omega r^2\dot{\theta}) = \\ &\qquad -2\frac{\Omega r^2}{U}f_2 \end{aligned}\right\} \quad \text{(B7)}$$

Note that the sin Ωt and cos Ωt no longer appear. Since these equations apply to a local section they must be integrated to establish the total resultant aerodynamic forces and moments at the propeller hub. The integration from hub to blade tip radius R leads to the following equations:

$$
\left.
\begin{aligned}
L_y &= \frac{1}{2}\rho V^2 S' \left(\frac{4\Omega^2 R c_0}{V^2} A_1' \psi - \frac{4\Omega c_0}{V} A_1 \frac{\dot{a}_1}{V} + \frac{4\Omega R}{V} A_2 \frac{\dot{\theta} c_0}{V} \right) \\
&= \frac{4\Omega^2 R^2}{{c_0}^2} 4M_a \left(\frac{c_0}{2} A_1' \psi - \frac{c_0}{2\Omega R} A_1 \dot{a}_1 + \frac{R c_0}{2\Omega R} A_2 \dot{\theta} \right) \\
L_z &= \frac{1}{2}\rho V^2 S' \left(\frac{4\Omega^2 R c_0}{V^2} A_1' \theta - \frac{4\Omega c_0}{V} A_1 \frac{\dot{b}_1}{V} - \frac{4\Omega R}{V} A_2 \frac{\dot{\psi} c_0}{V} \right) \\
&= \frac{4\Omega^2 R^2}{{c_0}^2} 4M_a \left(\frac{c_0}{2} A_1' \theta - \frac{c_0}{2\Omega R} A_1 \dot{b}_1 - \frac{R c_0}{2\Omega R} A_2 \dot{\psi} \right) \\
M_z &= \frac{1}{2}\rho V^2 S' R \left(\frac{4\Omega^2 R c_0}{V^2} A_2' \theta - \frac{4\Omega c_0}{V} A_2 \frac{\dot{b}_1}{V} - \frac{4\Omega R}{V} A_3 \frac{\dot{\psi} c_0}{V} \right) \\
&= \frac{4\Omega^2 R^2}{{c_0}^2} 4M_a R \left(\frac{c_0}{2} A_2' \theta - \frac{c_0}{2\Omega R} A_2 \dot{b}_1 - \frac{R c_0}{2\Omega R} A_3 \dot{\psi} \right) \\
M_y &= -\frac{1}{2}\rho V^2 S' R \left(\frac{4\Omega^2 R c_0}{V^2} A_2' \psi - \frac{4\Omega c_0}{V} A_2 \frac{\dot{a}_1}{V} + \frac{4\Omega R}{V} A_3 \frac{\dot{\theta} c_0}{V} \right) \\
&= -\frac{4\Omega^2 R^2}{{c_0}^2} 4M_a R \times \left(\frac{c_0}{2} A_2' \psi - \frac{c_0}{2\Omega R} A_2 \dot{a}_1 + \frac{R c_0}{2\Omega R} A_3 \dot{\theta} \right)
\end{aligned}
\right\} \quad \text{(B8)}
$$

where a value of $a = 2\pi$ is used. The alternate forms of the equations, involving a cylindrical mass of air about each blade and defined by $M_a = (\pi \rho {c_0}^2 R)/4$, have been given because of their convenience in whirl flutter considerations. The factors A_1, A_1', A_2, A_2', and A_3 in these equations are propeller functions defined by

$$
\left.
\begin{aligned}
A_1 &= \int_0^1 \frac{c}{c_0} \frac{(J/\pi)^2}{\sqrt{(J/\pi)^2 + \eta^2}}\, d\eta \\
A_1' &= (J/\pi) A_1 \\
A_2 &= \int_0^1 \frac{c}{c_0} \frac{(J/\pi)\eta^2}{\sqrt{(J/\pi)^2 + \eta^2}}\, d\eta \\
A_2' &= (J/\pi) A_2 \\
A_3 &= \int_0^1 \frac{c}{c_0} \frac{\eta^4}{\sqrt{(J/\pi)^2 + \eta^2}}\, d\eta
\end{aligned}
\right\} \quad \text{(B9)}
$$

These functions are noted to depend on the blade's chord geometry involving a reference chord c_0 and on the advance ratio J. For the case of a constant-chord propeller the integrals yield closed form results and give the values shown in Fig. 14.

Mach Number and Finite Blade-Length Effects

Tacit in the preceding derivation is the use of the theoretical lift-curve slope of 2π and incompressible flow. Compressibility and the induction effects of a finite-length blade may be taken into account approximately by modifying the lift-curve slope in some manner. One approach is to use a procedure often used in treating straight wings of finite aspect ratio, even though the wake shed by the propeller is helical in nature. For example, the lift-curve slope 2π may be multiplied by two factors, the Glauert-Prandtl Mach-number correction $1/\sqrt{1 - M_r^2}$, and a compressible-flow aspect-ratio correction $A'/(A' + 2)$, where M_r is the Mach number of the resultant velocity at each blade section and $A' = A\sqrt{1 - M_r^2}$, A being the blade aspect ratio. If this procedure is employed the resulting approximate overall correction to the lift-curve slope may be shown to be

$$
\frac{A}{2 + A\sqrt{1 - M_r^2}} = \frac{A}{2 + A\sqrt{1 - M^2\,[1 + (\pi^2/J^2)\eta^2]}} \quad \text{(B10)}
$$

where M is the forward-flight Mach number and $\eta = r/R$. To make use of this correction it is merely necessary to insert the factor (B10) under the integrals of the coefficients defined by Eqs. (B9) so that it forms part of the integrand.

Comparison With Ribner's Propeller Aerodynamics

The treatment of propeller whirl in Ref. 2 makes use of propeller aerodynamics based on the work of Ribner.[4] The correspondence of the propeller coefficients derived herein with the derivatives used in Ref. 2 can be obtained by comparing Eqs. (B8) of the present report with Eqs. (10) of Ref. 2. If this is done, the following results are found (taking into account the difference in sign convention):

$(4\Omega c_0/V)A_1$ corresponds to C_{Y_ψ} and $-C_{Z_\theta}$

$-(4\Omega c_0/V)A_2$ corresponds to C_{Y_q} and C_{Z_r}

$-(2\Omega c_0/V)A_2$ corresponds to C_{n_θ} and $-C_{m_\psi}$

$-(2\Omega c_0/V)A_3$ corresponds to C_{n_r} and C_{m_q}

As a numerical comparison of the results, consider the propeller treated in Ref. 2 for the case of $\beta_{0.75R} = 46°$, which corresponds to a value of $V/\Omega R = 0.75$. A comparison of the propeller derivatives as derived herein with those taken from Fig. 5 of Ref. 2 is given in Table 2. The second and third columns of this table are the result of applying the factor (B10) of the preceding section (using $M = 0$) to take approximate account of finite

TABLE 2

	Strip theory (Present report)	Strip theory × $\frac{A}{A+2}$		Reference 2
		A = 4.5 (No spinner)	A = 3.8 (With spinner)	
C_{Z_θ}	-0.73	-0.506	-0.478	-0.46
C_{Z_T}	-.281	-.195	-.184	-.19
C_{m_ψ}	.140	.097	.092	.10
C_{m_q}	-.106	-.073	-.07	-.073

blade-length effects. Quite favorable agreement is noted to occur when this is done.

Lift Lag due to Nonsteady Flow

Analogous to the case of an oscillating wing, the oscillatory lift which develops on the rotating-precessing propeller gives rise to a shed vortex which causes the lift to lag the quasi-steady value that is associated with the instantaneous angle of attack (the preceding sections represent the quasi-steady treatment). In the case of the propeller, however, the situation is much more complicated; first, for a four-bladed propeller there are four wakes causing induced effects; second, the wakes are helical; and, third, the wakes contain two frequency components (as will be seen shortly) due to the fact that the precession frequency is in general different than the rotating frequency. Rather than going into a rigorous treatment—which might, for example, involve the concept of helical "ladders" to represent the shed vortex sheet and trail—a greatly simplified consideration will be given to show the essential modifications to the lift that are brought about by wake effects. The derivation is found to substantiate the existence of a lift term that has been encountered in experiments with propellers, but which is not predicted by the foregoing quasi-steady development.

Thus, consider the lift equation (B4) and let the motion be represented by

$$f_1 = f_{10}e^{i\omega t}, \qquad f_2 = f_{20}e^{i\omega t}$$

The lift would then be given by

$$l_1 = -f_{10}e^{i\omega t}\frac{e^{i\Omega t} + e^{-i\Omega t}}{2} + f_{20}e^{i\omega t}\frac{e^{i\Omega t} - e^{-i\Omega t}}{2i}$$

which may be rearranged to

$$l_1 = -\tfrac{1}{2}(f_{10} + if_{20})e^{i(\Omega+\omega)t} - \tfrac{1}{2}(f_{10} - if_{20})e^{-i(\Omega-\omega)t}$$

This form shows that the lift and consequently the shed vortex contains two frequency components, one of frequency $\Omega + \omega$, the other of frequency $\Omega - \omega$. To take into account this wake, it is reasonable to expect that all wake effects may be accounted for approximately by introducing separate complex wake or circulation functions of the type conventionally used in the treatment of oscillating wings. A modified equation including lift lag effects would therefore appear

$$l_1' = -[(F_1 + iG_1)/2](f_{10} + if_{20})e^{i(\Omega+\omega)t} - [(F_2 - iG_2)/2](f_{10} - if_{20})e^{-i(\Omega-\omega)t} \quad \text{(B11)}$$

where the reduced frequency appropriate to the first term is defined by $k_1 = [(\Omega + \omega)c]/2U$, while $k_2 = [(\Omega - \omega)c]/2U$ applies to the second, where $U = \sqrt{V^2 + \Omega^2 r^2}$. Note the presence of the negative sign in $F_2 - iG_2$ is essential, since it may be shown that whereas an $(F + iG)$ term results from an assumed motion of $e^{i\omega t}$, an $(F - iG)$ occurs for a motion proportional to $e^{-i\omega t}$, where the G's are defined similarly (when Ω is considered to be greater than ω).

Now, if Eq. (B11) is reduced backward, the following equation is obtained:

$$l_1' = [(F_1 + F_2)/2](-f_1 \cos \Omega t + f_2 \sin \Omega t) + [(G_1 + G_2)/2](f_1 \sin \Omega t + f_2 \cos \Omega t) + [(G_1 - G_2)/2\omega](-\dot{f}_1 \cos \Omega t + \dot{f}_2 \sin \Omega t) - [(F_1 - F_2)/2\omega](\dot{f}_1 \sin \Omega t + \dot{f}_2 \cos \Omega t)$$

A similar treatment of l_3 [Eqs. (B5)] leads to

$$l_3' = [(F_1 + F_2)/2](f_1 \sin \Omega t + f_2 \cos \Omega t) - [(G_1 + G_2)/2](-f_1 \cos \Omega t + f_2 \sin \Omega t) + [(G_1 - G_2)/2\omega](\dot{f} \sin \Omega t + \dot{f}_2 \cos \Omega t) + [(F_1 - F_2)/2\omega](-\dot{f}_1 \cos \Omega t + \dot{f}_2 \sin \Omega t)$$

Use of Eqs. (B6) gives finally the following equations which "include" lift lag effects

$$l_y' = \frac{F_1 + F_2}{2}l_y + \frac{G_1 + G_2}{2}l_z + \frac{G_1 - G_2}{2\omega}\dot{l}_y - \frac{F_1 - F_2}{2\omega}\dot{l}_z$$

$$l_z' = \frac{F_1 + F_2}{2}l_z - \frac{G_1 + G_2}{2}l_y + \frac{G_1 - G_2}{2\omega}\dot{l}_z + \frac{F_1 - F_2}{2\omega}\dot{l}_y$$

It is interesting to see that the lag effect causes the quasi-steady lift l_y and l_z to be reduced in magnitude and to be turned through an angle $\phi = \tan^{-1}\frac{|G_1 + G_2|}{F_1 + F_2}$ in the direction of rotation. A side force due to pitch, or a vertical force due to yaw thus results, as has been found in tests on propellers. Note that average values of the F's and G's are involved in the first two terms of the lift expressions; this fact and the fact that ω is generally small compared with Ω suggests that the use of an F and G based on a reduced frequency $k = \Omega c/2U$, involving Ω alone, is probably sufficiently accurate for evaluating the amount of lag from a practical standpoint. Note also that the last two terms in the expressions involve differences of the F's and G's; the terms will therefore be quite small and probably are unimportant in practical applications.

References

[1] Taylor, E. S., and Browne, K. A., *Vibration Isolation of Air-*

craft Power Plants, Journal of the Aeronautical Sciences, Vol. 6, No. 2, pp. 43–49, Dec. 1938.

[2] Reed, W. H., III, and Bland, S. R., *An Analytical Treatment of Aircraft Propeller Precession Instability*, NASA TN D-659, Jan. 1961.

[3] Scanlan, R. H., and Truman, J. C., *The Gyroscopic Effect of a Rigid Rotating Propeller on Engine and Wing Vibration Modes*, Journal of the Aeronautical Sciences, Vol. 17, No. 10, pp. 653–659, 666, Oct. 1950.

[4] Ribner, H. S., *Propeller in Yaw*, NACA Rep. 820, 1945.

✦ ✦ ✦